Convergence Stability of Depth-Depth-Matching-Based Steepest Descent Method in Simulated Liver Surgery

Asano, Miho; Kuroda, Tomohiro; Numata, Satoshi; Jozen, Tuneo; Yoshikawa, Tomoki; Noborio, Hiroshi

International Journal of Pharma Medicine and Biological Sciences Vol. 10, No. 2, April 2021

Convergence Stability of Depth-Depth-Matching-Based Steepest Descent Method in Simulated Liver Surgery

Miho Asano[1], Tomohiro Kuroda[2,3], Satoshi Numata[4], Tuneo Jozen[4], Tomoki Yoshikawa[5], and Hiroshi Noborio[5]
[1]Preemptive Medicine and Lifestyle-Related Disease Research Center, Kyoto University Hospital, Kyoto, Japan
[2]Department of Social Informatics, Graduate School of Informatics, Kyoto University, Kyoto, Japan
[3]Division of Medical Information Technology and Administration Planning, Kyoto University Hospital, Kyoto, Japan
[4]Department of Digital Games, Osaka Electro-Communication University, Osaka, Japan
[5]Department of Computer Science, Osaka Electro-Communication University, Osaka, Japan
Email: {masano, tomo}@kuhp.kyoto-u.ac.jp, {numata, jozen, nobori }@osakac.ac.jp, ht16a095@oecu.jp

***Abstract*—We recently established that our digital potential function was globally stable at the point where a virtual liver coincided with its real counterpart. In particular, because three rotational degrees of freedom are frequently used in a surgical operation on a real liver, stability of the potential function concerning three rotational degrees of freedom was carefully verified in the laboratory, using fluorescent lamps and sunlight. We achieved the same stability for several simulated liver operations using a 3D printed viscoelastic liver in a surgical operating room equipped with two light-emitting diode shadowless lamps. As a result, with increasing number of lamps, stability of our depth-depth matching in the steepest descendent algorithm improved because the lamps did not emit an infrared spectrum such as the one emitted by our depth camera. Furthermore, the slower the angular velocity in a surgical sequence, the more overall stability improved.**

***Index Terms*—steepest descent method, virtual liver, actual liver, triangular polyhedron STL, liver surgery navigator, light-emitting diode shadowless lamps**

I. Introduction

Owing to high difficulty and complex anatomical characteristics, liver surgical navigation should be developed continuously to provide safe and accurate treatment. However, sensing accuracy of liver shape and motion remains problematic despite production of many excellent commercial cameras for real-time surgical navigation.

In contrast, Computed Tomography (CT), Magnetic Resonance Imaging (MRI), and Ultrasonography (US) have been used actively in surgery. In addition, many studies have been conducted to determine three-dimensional anatomy from obtained images and to detect organs and lesions [1]. The liver is a large organ containing several types of blood vessels. It is important to cause as little bleeding as possible when performing surgery. Because liver anatomy varies from person to person, a surgeon first examines preoperative images in detail and then performs a preoperative resection simulation, both of which are increasingly essential skills. Therefore, techniques for analyzing and applying medical images have advanced and are widely applied to surgical navigation to improve surgery safety.

Although many surgical navigation systems use 2- or 3D and ultrasound images [2], image resolution is low, and it is difficult to accurately detect actual liver position, direction, and shape. In addition, real-time navigation using projection mapping can project Indocyanine Green (ICG) light emission onto the hepatectomy surface, so although real-time navigation is possible, it cannot be projected into the deep surgical field [3]. The liver surgery navigator developed to solve these problems showed that a hybrid virtual whole liver including portal and arterial veins, a malignant tumor, and a nerve should overlap the real liver (i.e., liver replica) during simulated surgery. Therefore, we developed our depth–depth-matching-based steepest descendent method [4]-[7].

The algorithm generates some situations wherein a virtual liver quickly follows its real counterpart. In depth–depth matching, we always move the virtual liver to minimize the difference between depth images obtained from real and virtual livers. The real image can be captured by a depth camera such as Kinect v2. The virtual image automatically can be conveyed from the z-buffer of the virtual liver formed by the triangular polyhedron (STL) previously segmented by 3D Slicer from a patient's DICOM (Digital Imaging and COmmunications in Medicine) captured by CT/MRI.

Experiments were conducted in an operating room equipped with two Light-Emitting Diode (LED) shadowless lamps, simulating actual surgical lighting conditions. To determine influence of interference between infrared rays emitted from LED shadowless lamps and Kinect v2 on liver-tracking performance, we evaluated tracking performance of a virtual liver when its real counterpart was rotated and translated under lighting conditions generated using no LED shadowless lamps,

Manuscript received November 17, 2020; revised January 22, 2021.

doi: 10.18178/ijpmbs.10.2.60-67

one LED shadowless lamp, and two LED shadowless lamps. For rotational movement, we changed the velocity. For translation, when the initial liver position was adjusted, we evaluated tracking performance of either the whole liver or part of it and consequently determined differences in their tracking performances.

Section II describes experimental system components. In Section III, we describe our operating room and several experiments conducted therein, and we present experimental results. Section IV discusses significance of the main findings. Finally in Section V, we conclude by summarizing the main findings and their significance and provide direction for future research based on the findings of this study.

II. Experimental System Components

Herein, we introduce several components of our experimental system.

A. Virtual Liver

In this study, 3D Slicer was used to select a liver segment from a patient's DICOM taken before surgery, and a corresponding STL polyhedron was built as a virtual liver (Fig. 1).

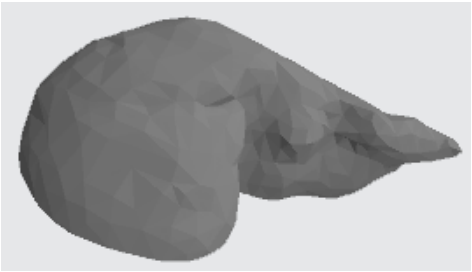

Figure 1. STL virtual liver model.

B. Actual Liver

From the STL liver model shown in Fig. 1, a concave plastic liver-shaped mold was constructed by a 3D printer, and human skin gel was poured into the mold to produce the viscoelastic liver model shown in Fig. 2. In this study, the viscoelastic liver model was assumed to be an actual liver during a simulated operation.

Figure 2. Human skin gel liver model.

C. Kinect for Windows v2

Fig. 3 shows Kinect v2, which captures depth images based on the Time-of-Flight (ToF) method, which measures many distances passing through many pixels to the target object by calculating the time that infrared rays reach the Kinect v2 image. Because the infrared ray emitted by Kinect v2 is modulated, it is not affected by ambient light when observing reflected light [8]-[11].

Figure 3. Kinect for windows v2.

D. iLED™ 7 Surgical Light (LED Shadowless Lamps)

The iLED™ 7 Surgical Light features automatically adjust several lighting conditions around a surgical site, using the latest 3D sensor technology. In addition, the shadow management system automatically compensates for unwanted shadows such as those projected by a surgeon's head, thereby ensuring excellent lighting at all times. Fig. 4 shows the iLED™ 7 surgical light. Table I lists corresponding technical data.

Figure 4. iLED™ 7 surgical light.

TABLE I. Technical Data for iLED™ 7 Surgical Light

Maximum central illumination (Ec) at 1 m	160,000 lx
Pattern size (d10) at 1 m	16–30 cm 6.3–11.8 inches
Color temperature	3,500 k/4,000 k/ 4,500 k/5,000 k
Average LED service life	60,000 h

E. Digital Logger

LX-2000SD is an illuminance meter that can measure illuminance and temperature. All the measured data can be recorded on an SD card. Fig. 5 shows the LX-2000SD digital data logger illuminometer, and Table II lists corresponding illuminance specifications.

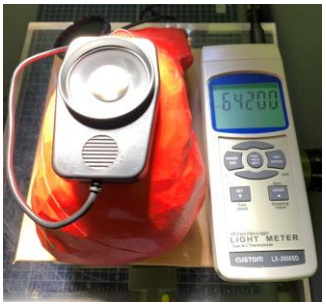

Figure 5. Digital data logger illuminance meter LX-2000SD.

TABLE II. TYPE SIZES FOR LX-2000SD

Range (lx)	Display range (lx)	Resolution (lx)	Measurement accuracy
2,000	0–1,999	1	± (4% rdg. + 2 dgt.)
20,000	1,800–19,990	10	
100,000	18,000–99,900	100	

F. Several Liver Surgery Navigator Windows

This section describes our liver navigator, which manually aligns initial positions of real and virtual liver depth images [7]. Fig. 6 shows several windows that control the liver surgery navigator. The operator displays a color image of the real liver (Fig. 6(a)), taken in real time with Kinect v2, and its corresponding depth image (Fig. 6(b)), and selects a region of the liver. The STL virtual liver is illustrated in the OpenGL window (Fig. 6(c)), and its corresponding depth image is shown in the OpenGL Depth window (Fig. 6(d)). Then, we adjust the Diff window so that the real-liver depth image displayed in Kinect Depth and the STL-virtual-liver depth image displayed in OpenGL Depth have the same position (Fig. 6(e)). The smaller the score (indicating the matching ratio of real- and virtual-liver depth images) displayed in the Kinect Depth window, the more the depth images of the real and virtual livers overlap [5]-[7]. The virtual liver then follows the movement of its real counterpart according to the algorithm.

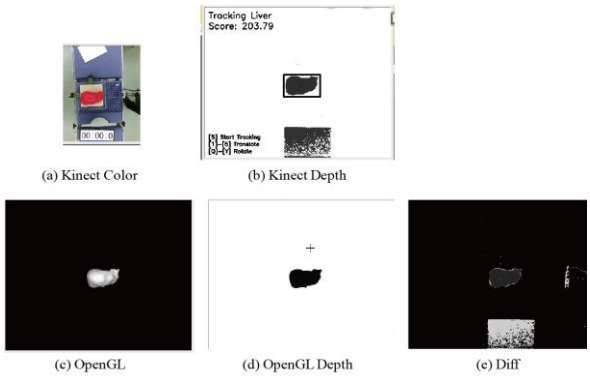

Figure 6. Liver surgery navigator windows.

G. Liver Tracking by Steepest Descent Method

Steepest descent is a well-known investigation algorithm for digital space. In our research, digital space is defined by 6 degrees of freedom of the 3D liver model (STL-polyhedron). Intuitively speaking, this is a method of optimizing the first derivative ($f'(x)$) of function $f(x)$; that is, updating points to more optimal ones by selecting the best neighbors around present points and then converging them to the best point in the digital 6D space, which consists of huge discrete points showing 3D rotational and translational degrees of freedom. First, we obtained an actual-liver depth image from Kinect v2 and compared it with that of its virtual counterpart to find the exact liver position and orientation. Accuracy is critically important for tracking liver status and displaying navigation information on a virtual liver. To improve accuracy, it is important to investigate how depth images of virtual and corresponding actual livers differ and to evaluate ability to track liver position and orientation [5], [6].

III. EXPERIMENTS CONDUCTED IN OPERATING ROOM EQUIPPED WITH LED SHADOWLESS LAMPS

Fig. 7 shows our surgical room, equipped with two LED lamps, where we investigated our depth–depth-matching-based algorithm by several experiments wherein we used a 3D-printed viscoelastic liver replica modeled from a patient's STL-polyhedron real liver. We placed the liver replica on a 0.25-m-long × 0.25-m-wide × 0.02-m-thick acrylic board on a rotating turntable and placed it on the operating table. The actual liver was moved by moving the acrylic board. By attaching Kinect v2 to a vertically movable robot, distance from the real liver could be changed. Kinect v2 was placed horizontal to the operating table, 0.9 m above the bottom of the real liver, and was fixed on a metal rod and attached to the vertical movement robot. Distance from the vertical robot to Kinect v2 was 0.32 m.

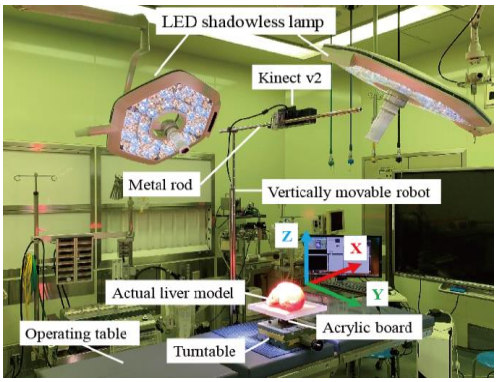

Figure 7. Operating room.

First, the real-liver-replica depth image was captured by Kinect v2, and the STL-polyhedron virtual-liver depth image was moved manually to align initial positions of the two images. The actual liver could be rotated 360° around the z-axis and translated 5 cm along the *x*-axis, as shown in Fig. 8. Accuracy was evaluated based on the matching index (which is the total match rate of the real- and virtual-liver depth images measured along the *x*-, *y*-, and *z*-axes) generated by adjustment from the initial position to the final rotation or translation position. Two previous papers [6] and [7] explain in depth how to calculate match rate.

The following paragraphs explain several experimental results obtained for real-liver rotation and translation under lighting conditions generated with no LED shadowless lamps, one LED shadowless lamp, and two LED shadowless lamps. Table III shows illuminance around the real liver during simulated surgeries.

TABLE III. ILLUMINANCE OF LED SHADOWLESS LAMP

	No LED shadowless lamps	One LED shadowless lamp	Two LED shadowless lamps
Illuminance [lx]	320	79,200	Exceeds display illuminance[a]

[a]Display illuminance: 0–99,000.

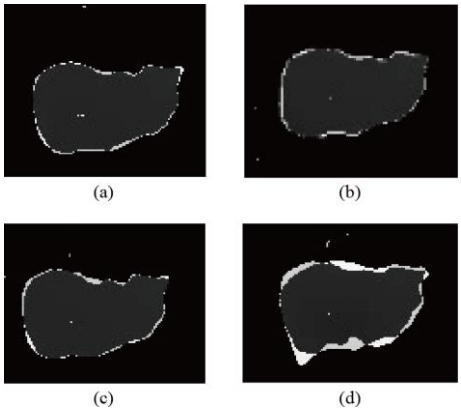

Figure 8. In operating room wherein LED shadowless lamps were turned off, virtual liver followed manually rotated real counterpart. Real-liver depth image (white) and virtual-liver depth image (black) are overlapped. Real- and virtual-liver depth images superimposed (a) before rotation and (b) after rotation at 6°/s and (c) before rotation and (d) after rotation at 9°/s.

A. Surgical Observation of Liver Rotation

Using the whole liver-shaped replica, initial positions of real- and virtual-liver depth images were aligned. The real liver was then manually rotated at 6, 9, or 18°/s, and its depth images were captured simultaneously in real time by Kinect v2. Our depth–depth-matching-based steepest descendent algorithm showed that the virtual liver automatically followed its real counterpart according to acquired depth-image data.

The first experiment was executed in a surgical operating room wherein LED shadowless lamps were turned off. When the real liver was manually rotated at 6°/s, the real and virtual livers rotated in tandem (Fig. 8). The second experiment was conducted in a surgical operating room wherein only one LED shadowless lamp was turned on. When the real liver was manually rotated at 9°/s, its virtual counterpart rotated in tandem (Fig. 9). The third experiment was performed in a surgical operating room wherein two LED shadowless lamps were turned on. When the real liver was manually rotated at 18°/s, its virtual counterpart rotated in tandem (Fig. 10).

As a result, in the operating room wherein LED shadowless lamps were turned off, when the real liver was rotated at 6 or 9°/s, its virtual counterpart followed, and the overlap ratio changed by ~200 on average and ~250 at worst or by ~300 on average and ~500 at worst, respectively. Therefore, with increasing angular velocity, the overlap ratio worsened during the simulated operation (Fig. 11(a) and Fig. 11(b)). In the operating room wherein only one LED shadowless lamp was turned on, when the real liver was rotated at 9 or 18°/s, its virtual counterpart followed, and the overlap ratio converged to ~1,000 by changing ~200 on average and ~300 at worst or by ~700 on average and ~1,400 at worst, respectively. Therefore, the overlap ratio worsened with increasing angular velocity during the simulated operation (Fig. 11(c) and Fig. 11(d)). In the operating room wherein two LED shadowless lamps were turned on, when the real liver was rotated at 18°/s, its virtual counterpart followed, and the overlap ratio converged to ~600 by changing ~700 on average and ~1,150 at worst during the simulated operation. Comparing depth images displayed in Fig. 9(d) with corresponding ones displayed in Fig. 10(b), liver-following convergence obtained using two LED lamps was considerably better than that obtained using only one.

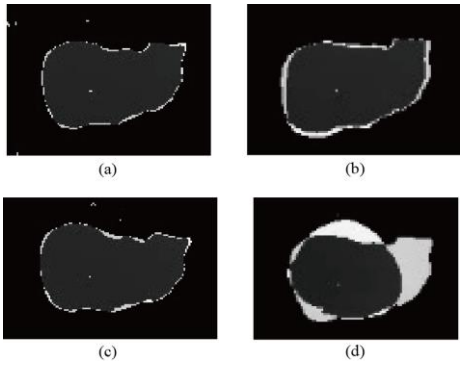

Figure 9. In operating room wherein only one LED shadowless lamp was turned on, virtual liver followed manually rotated real counterpart. Real-liver depth image (white) and virtual-liver depth image (black) are overlapped. Real- and virtual-liver depth images superimposed (a) before rotation and (b) after rotation at 9°/s and (c) before rotation and (d) after rotation at 18°/s.

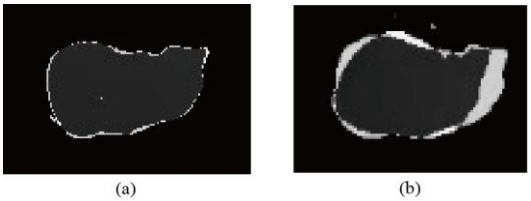

Figure 10. In operating room wherein two LED shadowless lamps were turned on, virtual liver followed manually rotated real counterpart. Real-liver depth image (white) and virtual-liver depth image (black) are overlapped. Real- and virtual-liver depth images superimposed (a) before rotation and (b) after rotation at 18°/s.

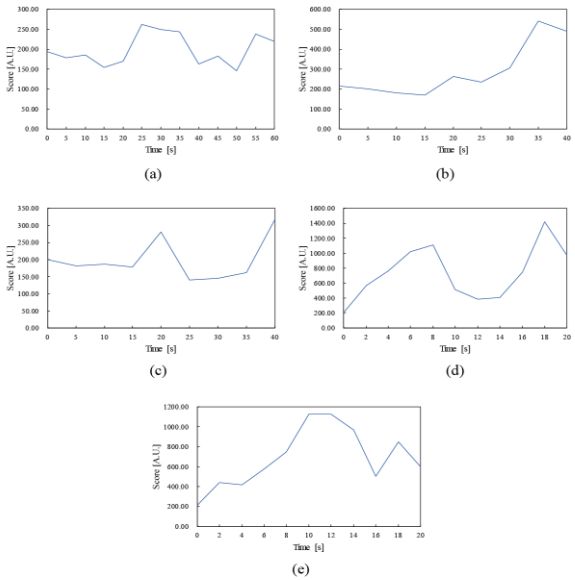

Figure 11. (a), (b) In operating room wherein LED shadowless lamps were turned off, virtual liver followed real counterpart manually rotated at 6 and 9°/s, respectively. (c), (d) In operating room wherein only one LED shadowless lamp was turned on, virtual liver followed real counterpart manually rotated at 9 and 18°/s, respectively. (e) In operating room wherein two LED shadowless lamps were turned on, virtual liver followed real counterpart manually rotated at 18°/s.

B. Surgical Observation of Liver Translation

Fig. 12 shows initial position alignments for real- and virtual-liver depth images of the whole liver and part of it. The real liver was manually translated, and its translation was always captured in real time by Kinect v2. According to our depth–depth-matching-based steepest descendent method, the virtual liver automatically followed its real counterpart, and translation velocity was constant.

Figure 12. Initial position alignments for real- and virtual-liver depth images of (a) whole liver and (b) part of liver.

The first experiment was conducted in a surgical operating room wherein LED shadowless lamps were turned off. The real and virtual livers moved parallel in tandem (Fig. 13(a), (b), (c), (d)). The second experiment was executed in a surgical operating room wherein only one LED shadowless lamp was turned on. The real and virtual livers moved parallel in tandem (Fig. 14(a), (b), (c), (d)). The third experiment was performed in a surgical operating room wherein two LED shadowless lamps were turned on. The real and virtual livers moved parallel in tandem (Fig. 15(a), (b), (c), (d)).

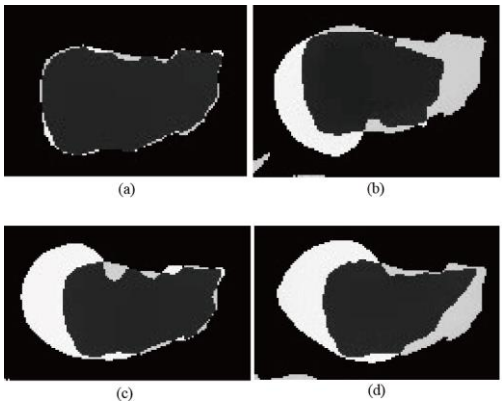

Figure 13. In operating room wherein LED shadowless lamps were turned off, virtual liver followed manually translated real counterpart. Real-liver depth image (white) and virtual-liver depth image (black) are overlapped. Real- and virtual-liver depth images superimposed (a) before and (b) after translation of whole liver and (c) before and (d) after translation of partial liver.

Accuracy of liver following in translation was evaluated based on depth images of the whole liver translated when zero, one, or two LED shadowless lamps were turned on, as shown in Fig. 16(a), Fig. 16(c), and Fig. 16(e), respectively. Furthermore, accuracy of liver following in translation was also evaluated based on depth images of a partial liver translated when zero, one, or two LED shadowless lamps were turned on, as shown in Fig. 16(b), Fig. 16(d), and Fig. 16(f), respectively. Initial position alignments for real- and virtual-liver depth images of whole and partial livers are shown in Fig. 12(a) and Fig. 12(b), respectively. Initially, average matching indices were about 1,200, 900, and 800 and the maximum matching indices were about 1,800, 1,300, and 1,200, as shown in Fig. 16(a), Fig. 16(c), and Fig. 16(e), respectively. Results suggested that accuracy of liver following in translation improved with increasing number of LED lamps. Furthermore, average matching indices were around 450, 300, and 200 and the maximum matching indices were around 700, 600, and 330 for a partial liver translated when zero, one, or two LED shadowless lamps were turned on, as shown in Fig. 16(b), Fig. 16(d), and Fig. 16(f), respectively.

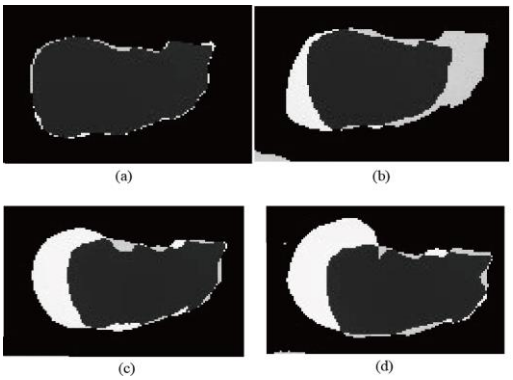

Figure 14. In operating room wherein only one LED shadowless lamp was turned on, virtual liver followed manually translated real counterpart. Real-liver depth image (white) and virtual-liver depth image (black) are overlapped. Real- and virtual-liver depth images superimposed (a) before and (b) after translation of whole liver and (c) before and (d) after translation of partial liver.

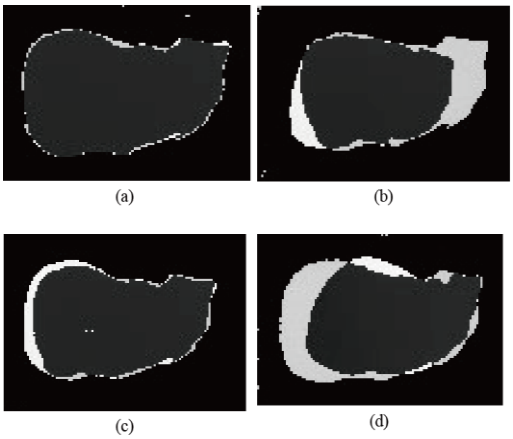

Figure 15. In operating room wherein two LED shadowless lamps were turned on, virtual liver followed manually translated real counterpart. Real-liver depth image (white) and virtual-liver depth image (black) are overlapped. Real- and virtual-liver depth images superimposed (a) before and (b) after translation of whole liver and (c) before and (d) after translation of partial liver.

These results suggest that liver-following accuracy improved with increasing number of LED lamps. Furthermore, the improvement was considerably more pronounced for a partial liver because the other part of the liver was quite flat. Therefore, the difference between real- and virtual-liver depth images was always less when the whole liver was translated.

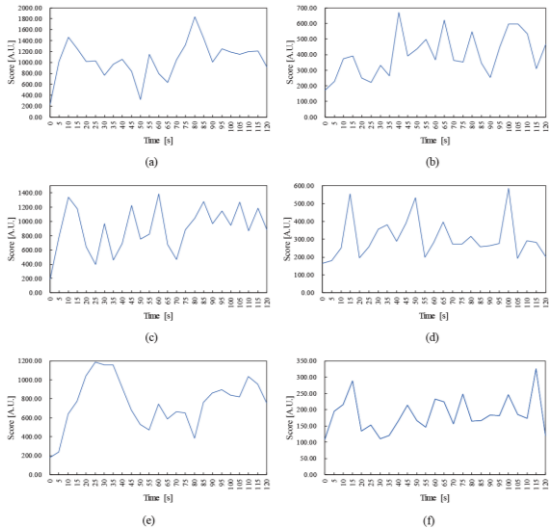

Figure 16. Matching indices obtained for liver following when whole liver was translated while (a) zero, (c) one, or (e) two LED shadowless lamps were turned on and when partial liver was translated while (b) zero, (d) one, or (f) two shadowless lamps were turned on. Initial position alignments for real- and virtual-liver depth images of whole and partial livers are shown in Fig. 12(a) and Fig. 12(b), respectively.

IV. Discussion

We verified convergence stability for depth–depth matching of steepest descent method under simulated surgical conditions. Experiments were executed in a surgical operating room equipped with two LED shadowless lamps. The main findings were as follows.

1) For the LED shadowless lamps used in the experiments, the virtual liver tracked its real counterpart more accurately in both rotation and translation with increasing number of lamps. In an experiment performed with filament or halogen shadowless lamps, infrared rays emitted from the shadowless lamp should be blocked using a sharp cut filter to prevent interference with infrared rays emitted from the depth sensor. However, we need not consider any such interference for a depth camera if we use LED shadowless lamps such as those used in these experiments.
2) In our algorithm, a virtual liver followed its real counterpart according to the difference between both depth images. Therefore, if a section of the liver is flat, the difference is always small even if both livers independently move. To achieve liver following, we should prepare a non-flat convex or concave shape around the livers to compare the whole liver and the convex part. As a result, liver-following achieved using only the convex part was more accurate than that achieved using the whole liver showing wide flat sections, which is especially advantageous for adjusting incisions of occluded liver parts in actual open liver surgery.
3) As shown in Fig. 10(b) and Fig. 11(e), a score of 600 after movement is the limit beyond which the depth images were no longer well overlapped. In other words, when the score was 0 to 600, the real liver and its virtual counterpart were strongly overlapped. However, our liver-following algorithm was limited owing to high angular velocity, as shown in Fig. 10(b) and Fig. 11(e). To overcome this limitation, we should improve sampling time of the depth sensor or increase velocity of the steepest descendent algorithm.

V. Conclusion

We used the depth–depth-matching-based steepest descent method to experimentally evaluate liver tracking during simulated liver surgery in an operating room equipped with LED shadowless lamps. Because the depth image of the real liver was not affected by the LED shadowless lamp, the more LED shadowless lamps, the more stable the depth–depth matching with the steepest descent algorithm. LED shadowless lamps did not emit any light spectrum that interfered with infrared rays emitted from the depth sensor. Therefore, increasing the number of LED shadowless lamps greatly improved liver-tracking accuracy. In addition, the slower the angular velocity, the more stable the convergence.

Moreover, using distinctive convex or concave features significantly improved liver-tracking accuracy. The liver showed few flat sections, and liver shape was greatly deformed by surgical excision, suggesting that our proposed liver surgery navigator is feasible for application to actual open liver surgery.

In future work, rotational and parallel translational movements will be performed mechanically, for which precise and stable operation evaluation will be required. Furthermore, to simulate actual surgical conditions, we must accurately evaluate our liver surgery navigation system using an incised real liver and its virtual counterpart occluded in an artificial human body.

Conflict of Interest

The authors declare no conflict of interest.

Author Contributions

Miho Asano, Tomohiro Kuroda, Satoshi Numata, Tsuneo Jozen and Hiroshi Noborio contributed to the research concept and design; Miho Asano, Tomohiro Kuroda, Satoshi Numata, Tsuneo Jozen and Hiroshi Noborio conceived the project and the study hypothesis; Miho Asano, Tomoki Yoshikawa and Hiroshi Noborio designed and participated in performing the experiments; Miho Asano, Satoshi Numata, Tomoki Yoshikawa and Hiroshi Noborio tested the software, analyzed the data; Miho Asano, Satoshi Numata executed implementation and evaluation of programming; Miho Asano analyzed the data; Miho Asano clearly wrote the paper by manuscript rewriting; all authors have approved the final version.

Acknowledgment

This study was supported partly by 2014 Grants-in-Aid for Scientific Research (No. 26289069) from the Ministry of Education, Culture, Sports, Science, and Technology,

Japan. Further support was provided by the 2014 Cooperation Research Fund from the Graduate School at Osaka Electro-Communication University. We would like to thank Editage (www.editage.com) for English language editing.

REFERENCES

[1] Y. Mise, K. Tani, T. Aoki, Y. Sakamoto, K. Hasegawa, *et al.*, "Virtual liver resection: Computer-assisted operation planning using a three-dimensional liver representation," *J. Hepatobiliary Pancreat. Sci.*, vol. 20, no. 2, pp. 157-164, Feb. 2013.

[2] S. Satou, T. Aoki, J. Kaneko, Y. Sakamoto, K. Hasegawa, *et al.*, "Initial experience of intraoperative three-dimensional navigation for liver resection using real-time virtual sonography," *Surgery*, vol. 155, no. 2, pp. 255-262, Feb. 2014.

[3] H. Nishino, E. Hatano, S. Seo, T. G. Nitta, T. Saito, *et al.*, "Real-time navigation for liver surgery using projection mapping with indocyanine green fluorescence: Development of the novel medical imaging projection system," *Ann. Surg.*, vol. 267, no. 6, pp. 1134-1140, June 2018.

[4] H. Noborio, S. Kiri, M. Kayaki, M. Koeda, and K. Onishi, "Accurate evaluation of rotational angle and translation movement of our organ-following algorithm based on depth-depth matching," in *Proc. 20th Int. Conf. Human-Computer Interaction: Interaction in Context*, Las Vegas, 2018, vol. 10902, part II, pp. 27-42.

[5] H. Noborio, K. Onishi, M. Koeda, K. Mizushino, M. Kaibori, *et al.*, "Motion transcription algorithm by matching corresponding depth image and z-buffer," in *Proc. 10th Anniv. Asian Conf. Comput. Aided Surg.*, Fukuoka, 2014, pp. 60-61.

[6] K. Watanabe, M. Yagi, K. Ota, K. Onishi, M. Koeda, *et al.*, "Parameter identification of depth-depth-matching algorithm for liver following," *Jurnal Teknologi*: *Med. Eng.*, vol. 77, no. 6, pp. 35-39, 2015.

[7] H. Noborio, K. Watanabe, M. Yagi, Y. Ida, K. Onishi, *et al.*, "Image-based initial position/orientation adjustment system between real and virtual livers," *Jurnal Teknologi*: *Med. Eng.*, vol. 77, no. 6, pp. 41-45, Nov. 2015.

[8] A. Procházka, M. Schätz, O. Vysata, and M. Valis, "Microsoft Kinect visual and depth sensors for breathing and heart rate analysis," *Sensors*, vol. 16, no. 7, p. E996, June 2016.

[9] A. Procházka, M. Schätz, F. Centonze, J. Kuchynka, O. Vysata, *et al.*, "Extraction of breathing features using MS Kinect for sleep stage detection," *Signal, Image and Video Process.*, vol. 10, no. 7, pp. 1279-1286, July 2016.

[10] M. K. Delimayanti, B. Purnama, N. G. Nguyen, K. R. Mahmudah, M. Kubo, *et al.*, "Clustering and classification of breathing activities by depth image from Kinect," in *Proc. Int. Joint Conf. Biomed. Eng. Syst. Technol.*, Prague, 2019, pp. 264-269.

[11] M. Schätz, F. Centonze, J. Kuchyňka, O. Ťupa, O. Vyšata, O. Geman, and A. Procházka, "Statistical recognition of breathing by MS Kinect depth sensor," presented at the International Workshop on Computational Intelligence for Multimedia Understanding, Prague, Czech Republic, Oct. 2015.

Miho Asano graduated from the Graduate School of Arts and Sciences, The Open University of Japan, Chiba, Japan and enrolled at the Graduate School of Engineering Science, Osaka University, Toyonaka, Japan from 2016 to 2018. Since 2016, Asano has been a research assistant at the Preemptive Medicine & Lifestyle-Related Disease Research Center of Kyoto University Hospital. She is interested in biomedical engineering, brain function measurement, national databases, and surgical navigation systems.

Tomohiro Kuroda received a B.S. in information science from Kyoto University, Japan in 1994, and an M.S. and a Ph.D. in information science from Nara Institute of Science and Technology, Japan in 1996 and 1998, respectively. He was with the Graduate School of Information Science at Nara Institute of Science and Technology, Japan from 1998 to 2001, where he held the rank of assistant professor, with the Department of Medical Informatics of Kyoto University Hospital, Japan from 2001 to 2006 and from 2009 to 2013, where he held the ranks of lecturer and associate professor, respectively, and with the Department of Information Processing Science at the University of Oulu, Finland in 2001 and 2006, where he held the rank of visiting professor. He was with the Graduate School of Engineering Science of Osaka University, Japan from 2007 to 2009, where he held the rank of associate professor. Since August 2013, he has been the director of the Division of Medical Information Technology and Administrative Planning (Chief Information Office) of Kyoto University Hospital, Japan, where he also serves as a professor of medical informatics in the Graduate School of Medicine and the Graduate School of Informatics. His current research interests include human interfaces, virtual/augmented reality, wearable/ubiquitous computing, and medical/assistive informatics. Dr. Kuroda is a member of IEEE, ISVR, VRSJ, HISJ, JSMBE, JAMI, JSMVR, ISCIE, JASL, and other prestigious organizations.

Satoshi Numata graduated from the Department of Engineering Informatics, Faculty of Engineering Informatics, Osaka Electro-Communication University, Osaka, Japan in 2000. He received a Dr. Information Science degree from the Graduate School of Information Science, Osaka University, Suita, Japan in 2005. He was a lecturer from 2005 to 2018, and he is currently an associate professor at the Department of Digital Games, Faculty of Information Science, Osaka Electro-Communication University. He is currently interested in programming education. Dr. Numata is a member of IPSJ, IEICE, JSSST, and JSISE.

Tsuneo Jozen graduated from the Department of Applied Mathematics and Physics, Kyoto University, Kyoto, Japan and received a Dr. Eng. degree from the Division of Environment Engineering, Graduate School of Engineering, Osaka University, Suita, Japan. From 2003 to 2006, he was a Visiting Assistant Professor at Kyoto University. From 2004, he joined Osaka Electro-Communication University. Professor Jozen has been the Dean of the Graduate School of Information Science and Arts at OECU since 2016. He is currently interested in surgical simulation and navigation. Dr. Jozen is a member of ACM, IPSJ, and IEICE.

Tomoki Yoshikawa is currently a student in the Department of Computer Science, Osaka Electro-Communication University, Osaka, Japan, where he is pursuing Bachelor's degree.

Hiroshi Noborio graduated from the Department of Computer Science, Shizuoka University, Hamamatsu, Japan and received a Dr. Eng. degree from the Department of Mechanical Engineering, Faculty of Engineering Science, Osaka University, Toyonaka, Japan. From 1987 to 1988, he was an Assistant Professor at Osaka University. In 1988, he became a lecturer at Osaka Electro-Communication University. Professor Noborio was Dean of the Faculty of Information Science and Arts at OECU from 2009 to 2012, and he is currently a Professor in the Department of Computer Science. He is currently interested in surgical simulation and navigation in the medical and dental fields. Dr. Noborio is a Member of IEEE, RSJ, SICE, IPSJ, and IEICE.